AFRL-SR-AR-TR-07-0378

REPORT DOCUMENTATION PAGE

1. REPORT DATE *(DD-MM-YYYY)*: 26-09-2007

2. REPORT TYPE: Final Report

3. DATES COVERED *(From - To)*: February 2004 - January 2007

4. TITLE AND SUBTITLE: Modeling Multiferroic Materials

5a. CONTRACT NUMBER:

5b. GRANT NUMBER: FA9550-04-1-0067

5c. PROGRAM ELEMENT NUMBER:

5d. PROJECT NUMBER:

5e. TASK NUMBER:

5f. WORK UNIT NUMBER:

6. AUTHOR(S)
Greg P. Carman
Gavin Chang
Grayson Bush

7. PERFORMING ORGANIZATION NAME(S) AND ADDRESS(ES)
The Regents of the University of California
Office of Contract and Grant Administration
11000 Kinross Ave, Suite 102; Box 951406
Los Angeles, CA 90095-1406

8. PERFORMING ORGANIZATION REPORT NUMBER:

9. SPONSORING/MONITORING AGENCY NAME(S) AND ADDRESS(ES)
Office of Naval Research
San Diego Regional Office
4520 Executive Drive, Suite 300
San Diego, CA 92121-3019
Dr Victor Giurgiutiu/NA

10. SPONSOR/MONITOR'S ACRONYM(S):

11. SPONSOR/MONITOR'S REPORT NUMBER(S):

12. DISTRIBUTION/AVAILABILITY STATEMENT
Approved for public release; distribution is unlimited.

13. SUPPLEMENTARY NOTES

14. ABSTRACT

The study's focus during the last three years was to analytically understand the effects of material properties as well as configurations on the magnetoelectric coupling in monolithic mangetoelectric materials and magnetostrictive/piezoelectric layered composites (denoted as MELC). The models generated during the last three years provide valuable information on understanding the magnetoelectric coupling behavior and hence maximized the magnetoelectric coupling for magnetoelectric system. The first part of the efforts had been devoted to developing continuum level models for both linear and nonlinear single phase magnetoelectric materials, including the solutions to representative problems. For the second effort, we focus on the MELC modeling. A total of six MELC configurations were studied by this model, including three field orientations, longitudinal, transverse, and in-plane, in both 1-D and 2-D plane geometries. By using the modeling analysis, a 3-D design map covering the span of compliance, Poisson's ratio, and piezomagnetic coefficient ratio of the magnetostrictive phases was generated.

15. SUBJECT TERMS
Magnetoelectric coupling in monolithic mangetoelectric materials, magnetostrictive/piezoelectric layered composites, MELC

16. SECURITY CLASSIFICATION OF: a. REPORT	b. ABSTRACT	c. THIS PAGE	17. LIMITATION OF ABSTRACT	18. NUMBER OF PAGES	19a. NAME OF RESPONSIBLE PERSON
					19b. TELEPHONE NUMBER *(Include area code)*

Standard Form 298 (Rev. 8/98)
Prescribed by ANSI Std. Z39.18

20071003424

Modeling Multiferroic Materials
FA9550-04-1-0067

Greg P. Carman, Gavin Chang, and Grayson Bush
Mechanical and Aerospace Engineering Department
University of California, Los Angeles
Los Angeles, CA 90095-1597
Voice: 310-825-6030
Fax: 310-206-2302
carman@seas.ucla.edu

ABSTRACT

The focus of the study during the last three years was to analytically understand the effects of material properties as well as configurations on the magnetoelectric coupling in monolithic mangetoelectric materials and magnetostrictive/piezoelectric layered composites (denoted as MELC). The models generated during the last three years provide valuable information on understanding the magnetoelectric coupling behavior and hence maximized the magnetoelectric coupling for magnetoelectric system. The first part of the efforts had been devoted to developing continuum level models for both linear and nonlinear single phase magnetoelectric materials, including the solutions to representative problems. For the second effort, we focus on the MELC modeling. A total of six MELC configurations were studied by this model, including three field orientations, longitudinal, transverse, and in-plane, in both 1-D and 2-D plane geometries. By using the modeling analysis, a 3-D α' design map covering the span of compliance, Poisson's ratio, and piezomagnetic coefficient ratio q_{33}/q_{31} of the magnetostrictive phases was generated. We also manufactured and tested several MELC systems with reasonable agreement between experiment and theoretical predictions.

ACHIEVEMENTS

Analytical Modeling

Monolithic Magnetoelectric Materials

This portion of the research focuses on developing new modeling capabilities for a heterogeneous layered thin film magnetoelectric and coupling these solutions with a new continuum model to predict the dynamic response. The first model, which is quasi-static, is used to understand the complex internal interactions intrinsic to monolithic magnetoelectric materials.

Initially a continuum level constitutive model was formulated for multiferroic materials using an energy approach. The linear model was used in the governing equations and a proof demonstrating uniqueness was obtained. The general formulation was applied to several standard problems, one of which is described below.

One analysis studied a rectangular sample of multiferroic material occupying a region of two-dimensional space denoted by $0 < x < l$ and $|z| \leq h$, as illustrated in Fig. 1 (b). The material has been polarized and magnetized through the thickness, i.e., parallel to the 3-direction or z-axis, and is assumed to be transversely isotropic in the 1-3 plane. The body is assumed to be in plane stress with constant field values in the width or 2-direction. On its boundaries, the material occupying the two-dimensional region described is subjected to uniform electric voltage ($\pm V_0$) as well as a uniform magnetic potentials ($\pm W_0$) at its top and bottom surfaces ($z = \pm h$), respectively. The material is subjected to a linearly varying stress (σ_x) through the thickness of the beam at the end, representing an applied moment at its ends ($x = 0$ and $x = l$).

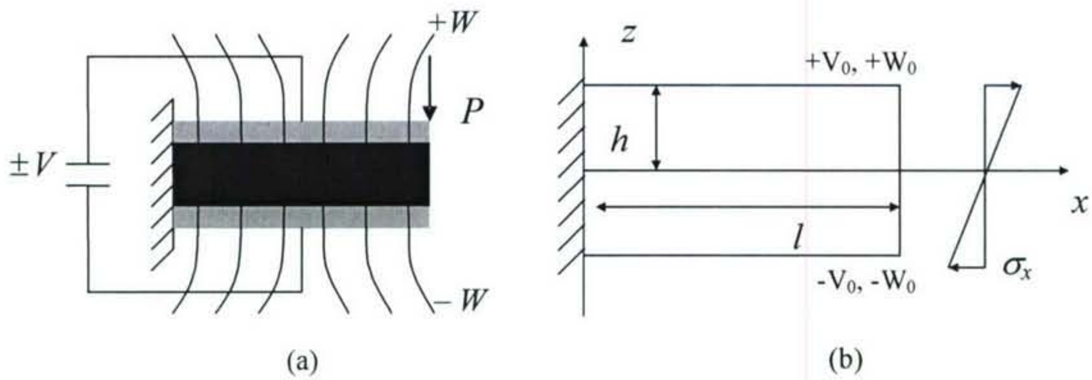

Figure 1. (a) Loading Scenario Considered for Analysis: A Two-Dimensional Beam Experiencing Combined Loading. (b) Loading Scenario Diagram.

Using the derived constitutive relations and the boundary value problem described above, relations describing the ability of the material to convert and store input energy or energies for the 31-directional case was computed. This came in the form of an effective coupling coefficients obtained through the analysis, given in Eq. 1 in terms of both material properties (1a) and the corresponding individual coupling coefficients (1b) for bipartite interactions.

$$k_{31,eff}^2 = \frac{\frac{d_{31}}{\sqrt{s_{11}\in_{33}}}\left(\frac{d_{31}}{\sqrt{s_{11}\in_{33}}} - \frac{q_{31}m_{33}}{\mu_{33}\sqrt{s_{11}\in_{33}}}\right) + \frac{q_{31}}{\sqrt{s_{11}\mu_{33}}}\left(\frac{q_{31}}{\sqrt{s_{11}\mu_{33}}} - \frac{d_{31}m_{33}}{\in_{33}\sqrt{s_{11}\mu_{33}}}\right)}{\left(1 - \frac{m_{33}^2}{\in_{33}\mu_{33}}\right)}$$

$$= \frac{k_{31,EE}\left(k_{31,EE} - k_{31,ME}k_{31,EM}\right) + k_{31,ME}\left(k_{31,ME} - k_{31,EE}k_{31,EM}\right)}{1 - k_{31,EM}^2} \qquad \text{(1a,b)}$$

The electro-magnetic coupling coefficient is of particular interest in this study. The square of the effective coupling coefficient ($k_{31,eff}$) when plotted as a function of the square of the electro-magnetic coupling coefficient ($k_{31,EM}$) reveals interesting information about the coupling behavior of the material. It can be seen in Fig. 2 that the maximum energy converted/stored (i.e., maximum $k_{31,eff}^2$) by the material system occurs at values of $k_{31,EM}$ close to zero and one. It is in this region of Fig. 2, where there is little transfer between electric and magnetic energies, and as a result the coupling exhibited in the material may be approximated by a superposition of piezoelectricity and piezomagnetism results.

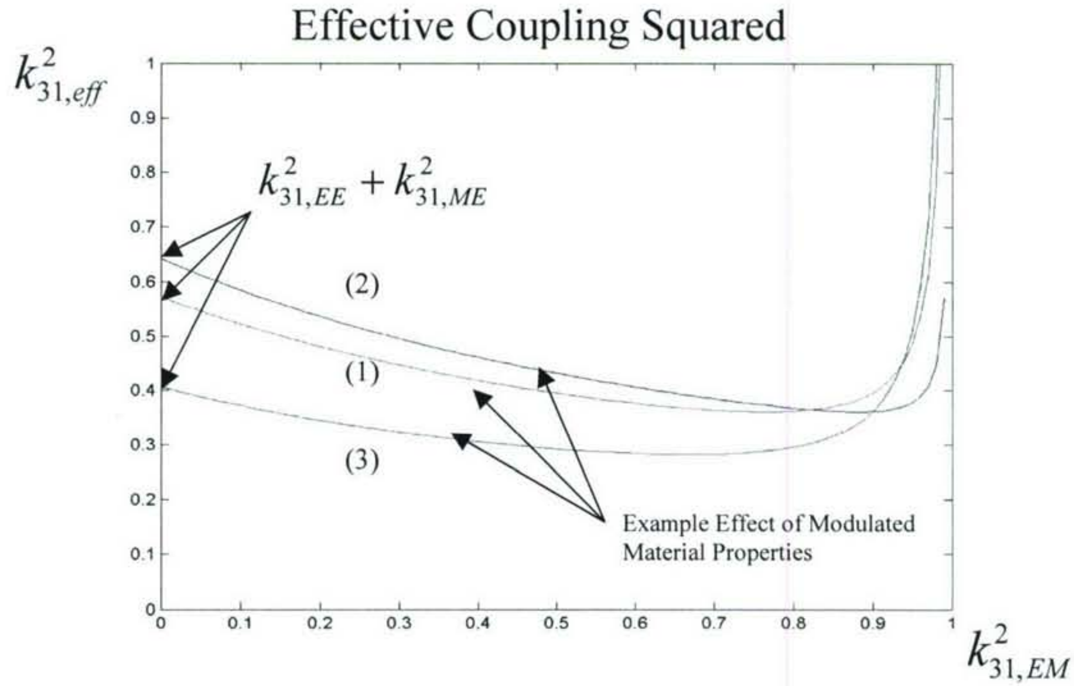

Figure 2. Effective Coupling Squared Plotted as a Function of Electro-magnetic Coupling Squared.

Magnetoelectric laminate composites (MELC)

In the program, a theoretical model was also developed for the predicting the magnetoelectric (M-E) voltage coefficient for a magnetostrictive/piezoelectric layered composite (MELC). Three field orientations; including longitudinal, transverse, and in-plane, with two in plane geometries, 2D and 1D, were studied with respect to the volume fraction of piezoelectric phase. As shown in Fig.3, three different field orientations are studied consisting of (i) poling direction and applied magnetic field being through the thickness (longitudinal mode, L); (ii) poling direction being through the thickness and magnetic field applied in-plane (transverse mode, T); and (iii) poling and applying magnetic field in-plane (in-plane mode, In). For each of these modes, 1D and 2D geometries are studied; thereby representing a total of six configurations. In discussing these cases, nomenclature of L2D, L1D, T2D, T1D, In2D, and In1D are used to denote the orientation (L, T, or In) and the geometry (1D or 2D). When a magnetic field is applied to each geometry, a deformation is generated in the magnetostrictive layer which is transmitted to the piezoelectric layer. This results in charge accumulation on the electrodes and an induced electric field in the piezoelectric layer. The magnetoelectric voltage coefficient α defined as δE/δH is used to predict magnetoelectric coupling effect as presented in the Fig.3.

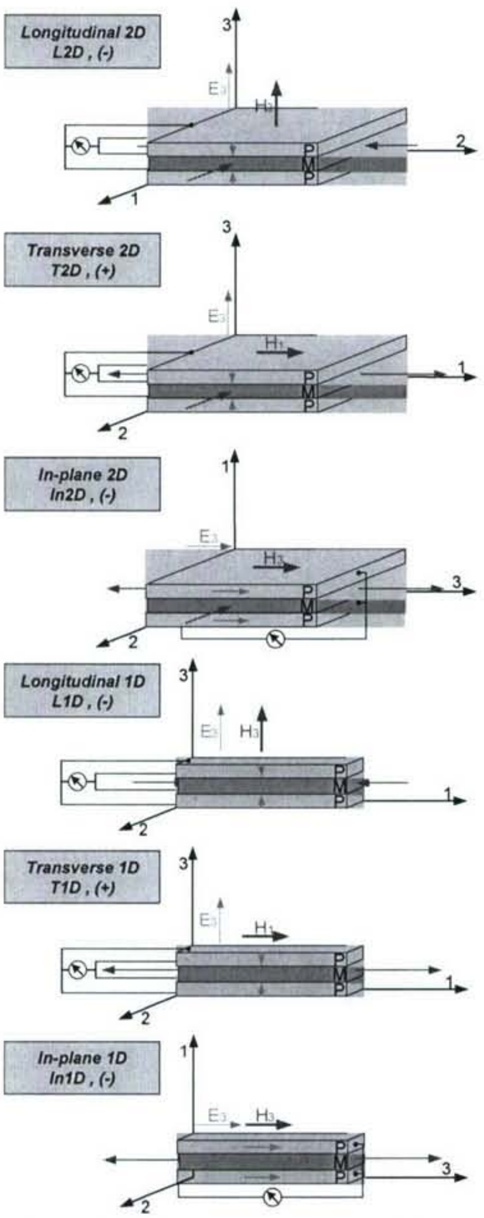

$$\alpha_{33}^{L2D} = \frac{E_3}{H_3} = \frac{-2\,{}^{p}d_{31}\,{}^{m}v\,{}^{m}q_{31}}{\left({}^{m}s_{11}+{}^{m}s_{12}\right){}^{p}v\in_{33}+\left({}^{p}s_{11}+{}^{p}s_{12}\right){}^{m}v\in_{33}-2\left({}^{p}d_{31}\right)^{2}\,{}^{m}v}$$

$$\alpha_{31}^{T2D} = \frac{E_3}{H_1} = \frac{-{}^{p}d_{31}\,{}^{m}v({}^{m}q_{11}+{}^{m}q_{12})}{\left({}^{m}s_{11}+{}^{m}s_{12}\right){}^{p}v\in_{33}+\left({}^{p}s_{11}+{}^{p}s_{12}\right){}^{m}v\in_{33}-2\left({}^{p}d_{31}\right)^{2}\,{}^{m}v}$$

$$\alpha_{33}^{In2D} = \frac{E_3}{H_3} = \frac{\begin{array}{c}{}^{m}v({}^{p}s_{33}\,{}^{p}d_{32}\,{}^{m}q_{32}\,{}^{m}v+{}^{p}s_{22}\,{}^{p}d_{33}\,{}^{m}q_{33}\,{}^{m}v-{}^{p}s_{23}({}^{p}d_{33}\,{}^{m}q_{32}+{}^{p}d_{32}\,{}^{m}q_{33})^{m}v\\ +({}^{m}s_{33}\,{}^{p}d_{32}\,{}^{m}q_{32}-{}^{m}s_{23}\,{}^{p}d_{33}\,{}^{m}q_{32}-{}^{m}s_{23}\,{}^{p}d_{32}\,{}^{m}q_{33}+{}^{m}s_{33}\,{}^{p}d_{33}\,{}^{m}q_{33})^{p}v)\end{array}}{\begin{array}{c}{}^{m}v({}^{p}s_{33}\,{}^{p}d_{32}^{\,2}\,{}^{m}v-2\,{}^{p}s_{23}\,{}^{p}d_{32}\,{}^{p}d_{33}\,{}^{m}v+{}^{m}s_{33}\,{}^{p}d_{32}^{\,2}\,{}^{p}v+{}^{p}d_{33}({}^{p}s_{22}\,{}^{p}d_{33}\,{}^{m}v\\ -2\,{}^{m}s_{23}\,{}^{p}d_{32}\,{}^{p}v+{}^{m}s_{33}\,{}^{p}d_{33}\,{}^{p}v))+(({}^{p}s_{23}^{\,2}-{}^{p}s_{22}\,{}^{p}s_{33})^{m}v^{2}-(-2\,{}^{m}s_{23}\,{}^{p}s_{23}\\ +{}^{m}s_{33}({}^{p}s_{22}+{}^{p}s_{33}))^{m}v\,{}^{p}v+({}^{m}s_{23}-{}^{m}s_{33})({}^{m}s_{23}+{}^{m}s_{33})^{p}v^{2})\in\end{array}}$$

$$\alpha_{33}^{L1D} = \frac{E_3}{H_3} = \frac{-{}^{p}d_{31}\,{}^{m}v\,{}^{m}q_{31}}{{}^{m}s_{11}\,{}^{p}v\in_{33}+{}^{p}s_{11}\,{}^{m}v\in_{33}-\left({}^{p}d_{31}\right)^{2}\,{}^{m}v}$$

$$\alpha_{31}^{T1D} = \frac{E_3}{H_1} = \frac{-{}^{p}d_{31}\,{}^{m}v\,{}^{m}q_{11}}{{}^{m}s_{11}\,{}^{p}v\in_{31}+{}^{p}s_{11}\,{}^{m}v\in_{31}-\left({}^{p}d_{31}\right)^{2}\,{}^{m}v}$$

$$\alpha_{33}^{In1D} = \frac{E_3}{H_3} = \frac{-{}^{p}d_{33}\,{}^{m}v\,{}^{m}q_{33}}{{}^{m}s_{33}\,{}^{p}v\in_{33}+{}^{p}s_{33}\,{}^{m}v\in_{33}-\left({}^{p}d_{33}\right)^{2}\,{}^{m}v}$$

Figure 3. Representative configurations with predictions of magnetoelectric voltage coefficients (α)

During the third year, a wide range of studies were conducted, varying the magnetostrictive material properties and the volume fraction of each configuration. This study enabled us to determine the individual effects of MELC configurations and magnetostrictive material properties on the homogenized M-E voltage coefficient, α', curves.

Material	s_{11} (10^{-12} m^2/N)	s_{12} (10^{-12} m^2/N)	s_{13} (10^{-12} m^2/N)	s_{33} (10^{-12} m^2/N)	q_{33} (10^{-12} m/A)	q_{31} (10^{-12} m/A)	d_{31} (10^{-12} m/V)	d_{33} (10^{-12} m/V)	$\varepsilon_{33}/\varepsilon_0$
PZT	16.1	-4.8	-8.5	20	-	-	-320	650	3800
CFO	6.5	-2.4			-1880	556	-	-	
NFO	6.5	-2.4			-680	125	-	-	
LSMO	15	-5			250	125	-	-	
C.TFD	86.9	-22.6			6389	-1614	-	-	

Table I Material parameters (compliance s, piezomagnetic coefficient q, piezoelectric coefficient d) for lead zirconate titanate (PZT), cobalt ferrite (CFO), nickel ferrite (NFO), lanthanum strontium manganite (LSMO), and composite Terfenol-D (C.TFD) are used for calculation

The effective properties used to predict the M-E coefficients are shown in Table 2. Figure 4 shows two plots, one for a CFO-PZT composite laminate and the other for a NFO-PZT laminate. Both figures plot the homogenized M-E voltage coefficient α' for the six cases as a function of PZT volume fraction ${}^{p}v$. The magnitude of α' ranges from 110.8 *mV/cm Oe* to 1037.0 *mV/cm Oe* for CFO-PZT and 24.9 *mV/cm Oe* to 375.3 *mV/cm Oe* for NFO-PZT. The larger α' values in the CFO-PZT system compared to NFO-PZT are attributed to the larger piezomagnetic coefficients. While the CFO-PZT system has larger α', the peak values arise at the same ${}^{p}v$, this is due to the same compliance values for CFO and NFO these two magnetostrictive materials.

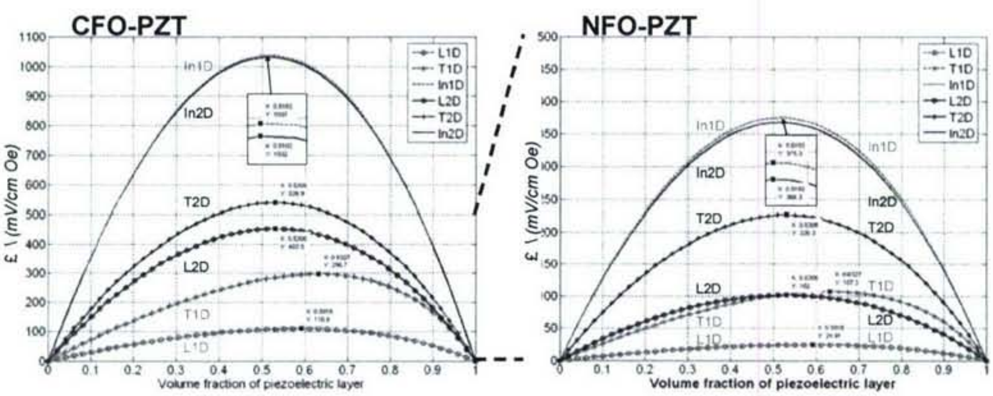

Figure 4. Homogenized M-E voltage coefficient α' for CFO-PZT and NFO-PZT as a function of volume fraction of piezoelectric phase

Another interesting feature at these graphs is the ordering of α'. That is, in the CFO-PZT system, the largest to smallest α' (i.e. In1D>In2D>T2D>L2D>T1D>L1D) occurs over the whole ${}^{p}v$ range; however, in NFO-PZT, the ordering changes with ${}^{p}v$. For ${}^{p}v$ less than 0.53, the ordering is In1D>In2D>T2D>L2D>T1D>L1D while for ${}^{p}v$ larger than 0.53, it is In1D>In2D>T2D>T1D>L2D>L1D. Since the two magnetostrictive materials, CFO and NFO, have the same compliance values, this change in ordering is attributed to piezomagnetic coefficient.

In order to investigate the effect of piezomagnetic coefficient further, both the piezomagnetic coefficient, q_{33}, but the ratio, q_{33}/q_{31} is considered. Figure 5 shows results for a CFO-PZT system with two different q_{33}/q_{31} ratios, i.e. -3.38 and -2.0. By comparing these two plots, we can see the largest to the smallest α' for each case changes. For q_{33}/q_{31}=-3.38, the sequence is In1D>In2D>T2D>L2D>T1D>L1D, while for q_{33}/q_{31}=-2.0 the sequence is In2D>In1D>L2D>T2D>T1D>L1D. It is worth noticing the largest value α' changes from In2D to In 1D. Furthermore, L2D dramatically surpasses T2D for the ratio q_{33}/q_{31}=-2.0 while T2D is larger than L2D for the ratio q_{33}/q_{31}=-3.38. By referencing to Figure 1 and equations L2D and T2D, we conclude that increasing the ratio q_{33}/q_{31} significantly improve the M-E coupling for L2D case but counteracts T2D response. The result is also in agreement with the M-E effect measurement in L2D type sample studied by Ryu which reaches the highest M-E coupling (4.68×10^{3} *mV/cm Oe*) for the L2D when compared to the T2D configurations.

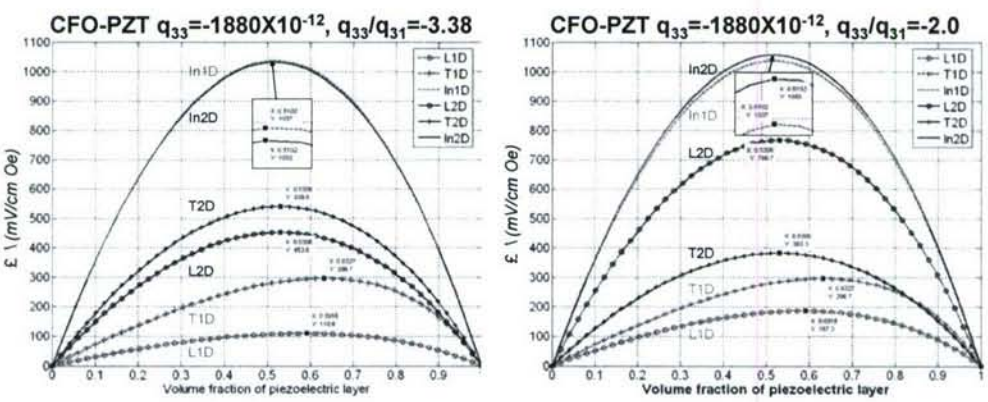

Figure 5. Comparison of homogenized M-E voltage coefficient α' for CFO-PZT under the different ratio q_{33}/q_{31}(-3.38 v.s.-2.0)

On the contrary, if the q_{33}/q_{31} ratio is fixed while only q_{33} value is changed, we can study the effects of q_{33} on α'. As shown in Fig. 6, by increasing the q_{33} of NFO from -680×10^{-12} *m/A* to -800×10^{-12} *m/A*, the peaks of each configurations increase roughly by a factor of 1.15 without changing sequence. Therefore, given the same compliance properties, the ordering of α' for each case is influenced by the ratio q_{33}/q_{31} instead of the q_{33} value.

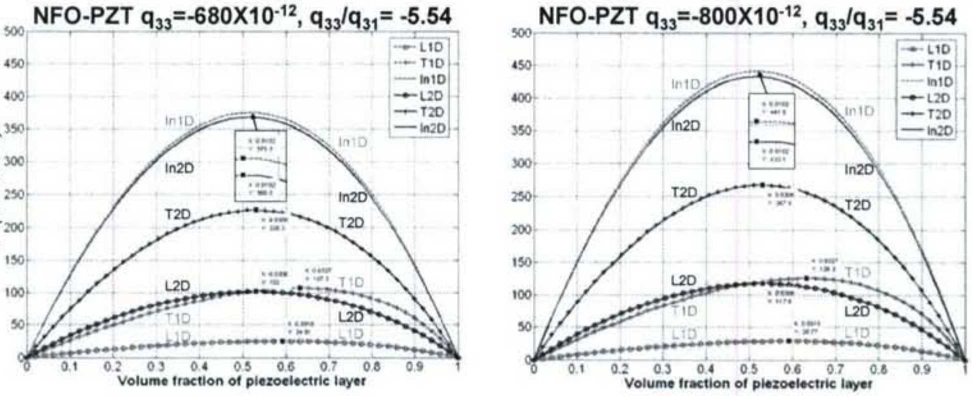

Figure 6. Comparison of homogenized M-E voltage coefficient α' for NFO-PZT under the different piezomagnetic coefficient q_{33} (-680×10^{-12} m/A v.s. -800×10^{-12} m/A)

To study the influence of compliance property, comparison of LSMO and composite Terfenol-D (Terfenol-D particulate mixed with resin) are presented in Fig. 7. LSMO-PZT exhibits a low α' ranging from 16.2 *mV/cm Oe* to 90.1 *mV/cm Oe* while the Terfenol-D composite α' ranges from 73.0 *mV/cm Oe* to 676.4 *mV/cm Oe*.

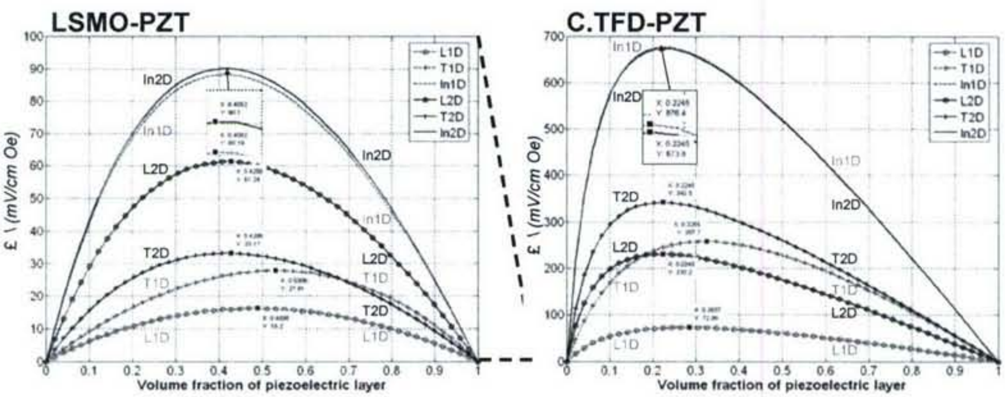

Figure. 7 Homogenized M-E voltage coefficient α' for LSMO-PZT and Composite Terfenol-D-PZT (C.TFD-PZT) as a function of volume fraction of piezoelectric phase

By comparing the peak values of L2D in LSMO-PZT to NFO-PZT, we can see LSMO-PZT is lower by a factor of 2 (61.24 *mV/cm Oe* for LSMO-PZT and 102 *mV/cm Oe* for NFO-PZT). However, as shown in Table1, the magnetostrictive property q_{31} are the same for LSMO and NFO but different compliance (LSMO's is about 2 times higher than NFO's). Because α' of L2D is affected solely by q_{31} as shown in Fig.3, the weak α' is attributed to high compliance and not piezomagnetic coefficient. Further comparison is obtained from the composite Terfenol-D-PZT. With about 25 times higher piezomagnetic coefficient (q_{33}=6,389$\times10^{-12}$ *m/A* for composite Terfenol-D) compared to q_{33} of LSMO (250×10^{-12} *m/A*), the α' peak of In1D case (solely affected by q_{33}) only exhibits 8 times larger magnitude. We conclude that, as the compliance further increases, not only the magnitude of α' decreases but α' peaks shift to smaller values of ${}^{p}v$. This suggests that mechanical impedance matching is an important property to maximize α'.

Results show that the piezoelectric phase volume fraction to achieve maximum M-E coupling effect is dependent upon the compliance of magnetostrictive phase. Higher compliance values shift α' peaks to lower piezoelectric volume fraction and attenuate α' values. This study also investigated the influence of the piezomagnetic coefficient q_{33} and the ratio q_{33}/q_{31} on α'. For constant ratio of q_{33}/q_{31}, larger q_{33} values increase the M-E coupling effect. However, changing this ratio alters the relative ordering of the α' values for each of the six MELC configurations studied. This demonstrates that the ratio q_{33}/q_{31} strongly influences the selection of MELC configurations to produce the largest M-E coupling effect.

Using the results from this modeling analysis, a 3-D α' sequencing map, as shown in Fig. 8, covering the span of compliance, Poisson's ratio, and piezomagnetic coefficient ratio q_{33}/q_{31} of the magnetostrictive phase can be generated to aid in the designing MELC system. Each surface presented in the map represents a transition boundary from one sequence to another, i.e. a transition plane on which α' values of two configurations are equivalent. For the region between surfaces, we have provided the sequencing that is produced for each particular region. The order of the α' values from the largest to the smallest is hence clearly illustrated in the magnetostrictive material property space. As can be seen, the MELC configuration with the maximum α' value changes as the properties of the material changes. Therefore, it is incorrect to assume a given configuration always exhibits the highest α' value. Fig. 8 can also be used by researchers, manufacturers, and designers to select geometries and field orientation for MELC systems that achieve the highest magnetoelectric effect based on the choice of magnetostrictive phase properties. Furthermore, if we consider the variety of magnetostrictive material properties in MEMS fabrication process, this mapping can also be employed to determine expected response from a wide range of material selection and process setting.

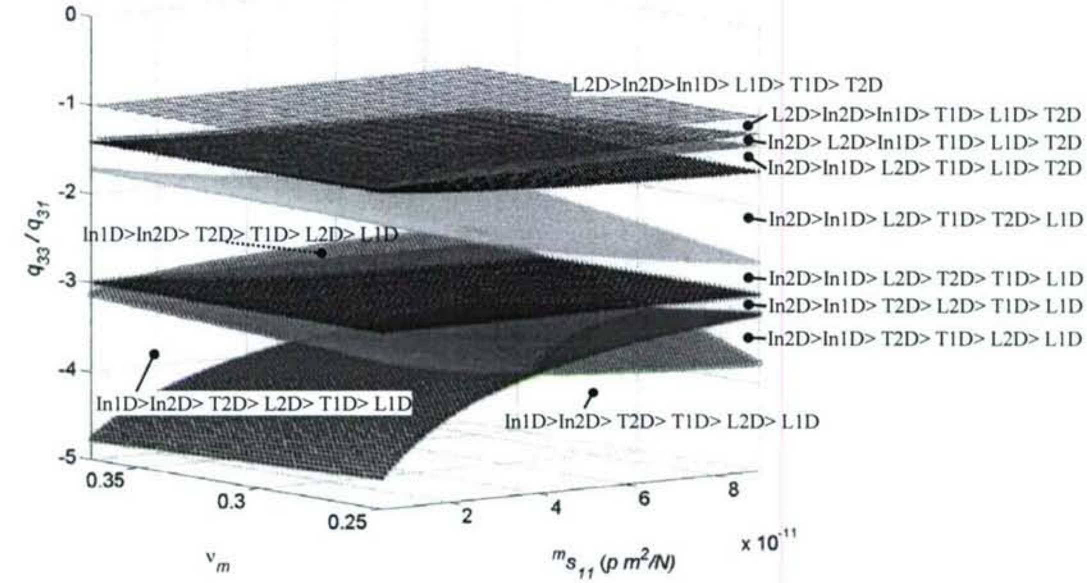

Figure. 8 3-D α' sequencing map covering the span of compliance ${}^{m}s_{11}$, Poisson's ratio ν_m, and piezomagnetic coefficient ratio q_{33}/q_{31} of the magnetostrictive phases

Fabrication and Experiment

A Terfenol-D layer used in the magneto-electric laminate composite consisted of aligned Terfenol-D particulates and a polymer resin. The fabrication process for the Terfenol-D layer is shown in Fig. 9. The 1-3 Terfenol-D composites were fabricated by mixing 55% by volume ball-milled, 50~300 μm in size, Terfenol-D particulates (ETREMA Products, Inc., Ames, IA) with a Vinyl ester resin (Dow Derakane 411-C50) in a Plexiglas mode with a cavity of 24.45×14.45×12.55 mm^3. The mixtures were degassed to eliminate the voids inside the composite and the liquid slurry was placed between a pair of Nd-Fe-B permanent magnets producing a magnetic field of 150 kA/m to align the particulates. The composite was then placed in a vacuum oven at 70 °C for 8 hours to fully cure the Vinyl ester resin. Fig. 9(a) shows the Terfenol-D composite after demolding.

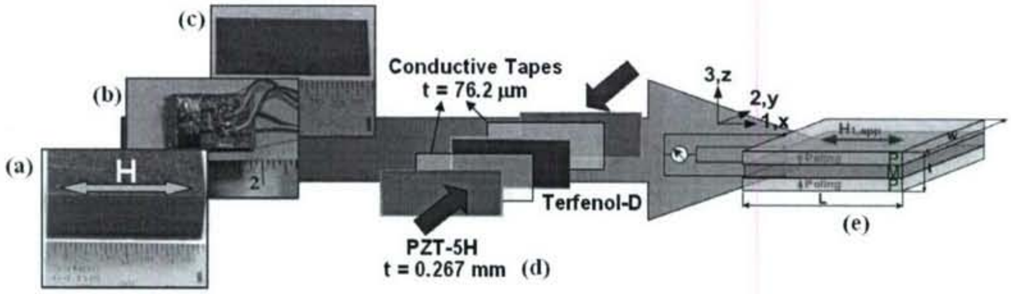

Figure 9. (Color online) 1-3 Terfenol-D and Magneto-Electric samples fabrication

The Terfenol-D composite shown in Fig. 9(b) was characterized to obtain material properties including elastic moduli (${}^{m}Y_{11}$, ${}^{m}Y_{22}$), piezomagnetic coefficients (${}^{m}q_{11}$, ${}^{m}q_{12}$), and relative permeability (μ_r) for various mechanical loadings as a function of a bias magnetic field. The data is important to ensure that variations observed between test data and theory are not the result of inaccurate properties used in the models. Two different sets of measurements were conducted at room temperature. The first set of tests involved applying a bias magnetic field (H_{bias}) and a compressive bias mechanical preload (σ_{bias}) in a presence of a time-varying mechanical loading ($\sigma_{1,ac}$). A sinusoidal $\sigma_{1,ac}$ of 2 MPa amplitude was applied at 0.3 Hz to characterize the elastic modulus for σ_{bias} combinations ranging from 2 MPa to 12 MPa in 2 MPa increments with H_{bias} ranging from 0 Oe to 4000 Oe in 500 Oe increments. The second set of tests applies a compressive σ_{bias} with a time-varying $H_{1,ac}$. A σ_{bias} ranging from 0 MPa to 12 MPa in 2 MPa increments was applied followed by a sinusoidal $H_{1,ac}$ with amplitude of 4000 Oe at 0.3 Hz. For both sets of tests, data was recorded for 7 cycles and average material properties were calculated with trivial statistical deviation.

Following characterization, the composite was sliced into laminates of three thicknesses of 0.69 mm, 1.34mm, and 2.62 mm with the same 24.45×12.55 mm^2 planar area as shown in Fig. 9(c). The piezoelectric ceramic in the magnetoelectric (M-E) laminate composite is a PZT-5H plate of 0.27 mm×24.5 mm×12.6 mm (Piezo Systems, Inc., Cambridge, MA). As illustrated in Fig. 9(d), each M-E laminate was fabricated by sandwiching a single layer of Terfenol-D composite laminate between two oppositely poled PZT-5H plates with a 76 μm thick silver conductive tape for bonding. These three M-E laminates were cured at 125 °C for 2 hours under a 30 psi compression resulting in M-E laminates of various piezoelectric volume fractions, ${}^{p}v$, of 0.44, 0.29, and 0.17. The piezoelectric layers were electrically connected in parallel, Fig. 9 (e), to monitor the voltage/charge produced.

We fabricated a number of symmetric MELCs. Fig. 10 shows a sample of the fabricated laminates for T2D in Figure 1. The magnetoelectric laminates were fabricated by sandwiching a layer of 1-3 Terfenol-D particulate composite in between two layers of PZT-5H to eliminate the bending of the MELC. The layers were bonded using a conductive tape with a thickness of 25 – 50 μm (Emerson & Cuming CF3350). The MELC were cured at 137 °C for 1 hour under a 50 psi compression to ensure good mechanical bonding between layers. The Terfenol-D layers of different thickness, a total five piezoelectric volume fractions, defined as the thickness ratio of PZT-5H to the MELC, were obtained with ${}^{P}v$ of 0.17, 0.28, 0.34, 0.38, and 0.44. To conduct high frequency tests, the magnetostrictive layers were fabricated with Terfenol-D particulates of 50 μm ~300 μm in size embedded into a vinyl ester resin matrix (Dow Derekane 411-C50).

$${}^{P}v = \frac{\text{Thickness of PZT}}{\text{Total Thickness of MPLC}}$$

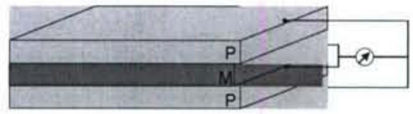

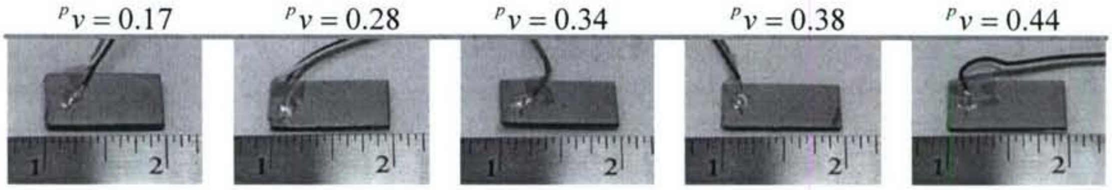

Figure 10. Illustration and pictures depicting the different magnetoelectric laminates manufactured

Fig. 11 compares the theoretical and experimental magnetoelectric voltage coefficient (α) for MELC systems with the volume fraction of 0.2, 0.4, and 0.8. The solid symbols mark the experimental results and the hollow symbols with dashed lines represent the theoretical predictions. All the α curves for each sample show similar trend which increase to the peak value and decrease with the bias magnetic field. Furthermore, for the case of ${}^{P}v$=0.2, the theoretical and experimental α's reach the identical values of around 1 V/cm-Oe with the error less than 2 %. This provides researchers a viable method to estimate the experimental magnetoelectric responses by using theoretical prediction. Although the results are promising, there is a deviation for the other cases. As the piezoelectric volume fraction increases, the differences between the test and theory become more significant. This complex but interesting phenomenon is proposed to be caused by the stress transmission lag due to the coupling magnetostrictive/piezoelectric interface and the demagnetization of the magnetostrictive layer.

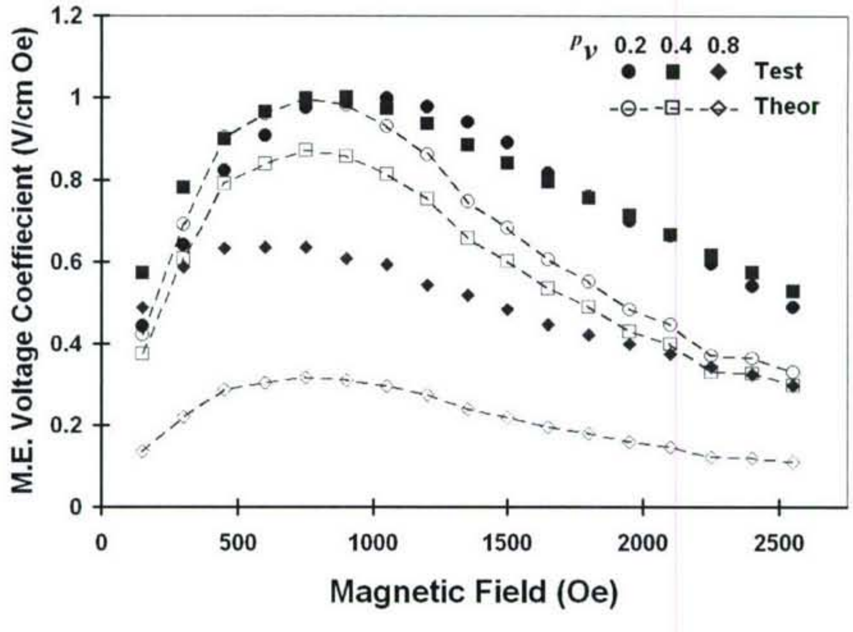

Figure 11. The theoretical and experimental magneotelectric voltage coefficient (α) for magnetoelectric laminate composites (MELC) with piezoelectric volume fraction of 0.2, 0.4, and 0.8. Solid and hollow symbols represent test and theory results, respectively.

PAPERS PUBLISHED UNDER CONTRACT

Bush, G & Carman G.P., "Electromagnetically-Coupled Plane Waves In Linear Multiferroic Waves in Linear Multiferroics" International Journal of Mechanics and Materials in Design (2007) accepted for publication.

Chia-Ming Chang and Gregory P. Carman, "Analytically evaluating the properties and performance of layered magnetoelectric composites", Journal of Intelligent Material Systems and Structures, 2007, accepted for publication.

Ujihara, M., Lee, D.G., and Carman, G.P, "Thermal Energy Harvesting Device Using Ferromagnetic Materials," Applied Physics Letters, 91:093508 - 093511 (August 2007)

Nersessian, N., Or, S.W., Carman, G.P., Choe, W., Radousky, H.B., McElfresh, M.W., Pecharsky, V.K., Pecharsky, A.O., "$Gd_5Si_2Ge_2$ Composite for Magnetostrictive Actuator Applications", *Applied Physics Letters*, V. 84, #23, 4801-4803.

Nersessian, N., Or, S.W., and Carman, G.P., "Magnetoelectric Laminates of Terfenol-D Composite and Lead Zirconate Titanate Ceramic Laminates", *IEEE Transactions on Magnetics*, V 40, no 4, July 2004. pp 2646-2648

Grayson B and Carman G.P., "The Analysis of Linear Ferroelectro-Magnetic Continua and Their Couplines" *Integrated Ferroelectrics*, V71,2005, pp. 181-191.

C. M. Chang and G. P. Carman, "Modeling of Coupling Effect in Magneto-Electric Layered Composites" in Smart Structure and Integrated Systems, *Proceedings of the International Society for Optical Engineering*, 6173, 617317, San Diego, 2006

Bush, G. J., Carman, G. P., "The Analysis and Effective Coupling of Linear Ferroelectro-magnetic Continua," in Smart Structure and Integrated Systems, *Proceedings of the International Society for Optical Engineering*, vol.5387, no.1, 2004, pp. 302-13,. USA

HONORS AND AWARDS

Adaptive Structures and Material Systems Prize, 2004, Greg P. Carman
Fellow ASME, 2003, Greg P. Carman
Honorary Professor Baotou University of Iron and Steel Technology, China, 2002, Greg P. Carman